Nanoscale

Accepted Manuscript

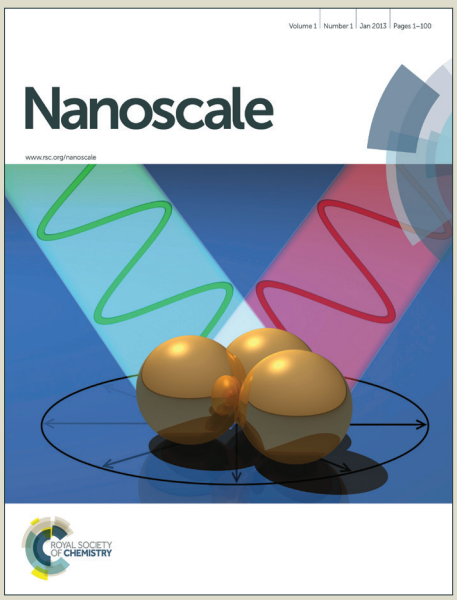

ROYAL SOCIETY OF CHEMISTRY

www.rsc.org/nanoscale

Journal Name

RSCPublishing

ARTICLE

In-situ growth of capping-free magnetic iron oxide nanoparticles on liquid-phase exfoliated graphene

Cite this: DOI: 10.1039/x0xx00000x

T. Tsoufis,[a*] Z. Syrgiannis,[b] N Akhtar,[a] M. Prato,[b*] F. Katsaros,[c] Z. Sideratou,[c] A. Kouloumpis,[d] D. Gournis,[d] and P. Rudolf,[a*]

Received 00th February 2015,
Accepted 00th February 2015

DOI: 10.1039/x0xx00000x

www.rsc.org/

We report a facile approach for the *in-situ* synthesis of very small iron oxide nanoparticles on the surface of high-quality graphene sheets. Our synthetic strategy involved the direct, liquid-phase exfoliation of highly crystalline graphite (avoiding any oxidation treatment) and the subsequent chemical functionalization of the graphene sheets via the well-established 1,3-dipolar cycloaddition reaction. The resulting graphene derivatives were employed for the immobilization of the nanoparticle precursor (Fe cations) at the introduced organic groups by a modified wet-impregnation method, followed by interaction with acetic acid vapours. The final graphene-iron oxide hybrid material was achieved by heating (calcination) in an inert atmosphere. Characterization by X-ray diffraction, transmission electron and atomic force microscopy, Raman and X-ray photoelectron spectroscopy gave evidence for the formation of rather small (<12 nm), spherical, magnetite-rich nanoparticles which were evenly distributed on the surface of few-layer (<1.2 nm thick) graphene. Due to the presence of the iron oxide nanoparticles, the hybrid material showed a superparamagnetic behaviour at room temperature.

1. Introduction

The discovery in 2004 that graphene can be produced by micromechanical exfoliation[1] brought forth a plethora of unique electronic, mechanical, thermal and optical properties of this first stable two dimensional (2-D) material ever isolated.[2] To harness these properties for applications many efforts target alternative chemical strategies for the large scale production of graphene. Graphene oxide (denoted hereafter as *GO*) produced via methods which involve the oxidative treatment of graphite to various levels,[3,4] was initially considered a very attractive graphene chemical derivative. But it was soon realized that GO sheets suffer from severe structural damage (i.e. exhibit topographical defects introduced along their two-dimensional graphitic framework).[5] The introduced structural damage is strongly reflected to the physicochemical properties of the derived GO resulting in a material which is conceptually different from graphene. A characteristic example is the electrical conductivity; while high-quality graphene sheets exhibit an excellent conductive behaviour.[6,7] GO is an insulator.[8] In an effort to overcome these drawbacks, a treatment commonly known as reduction of GO was proposed. However the production of reduced GO (denoted hereafter as r-GO) requires an additional chemical treatment step and most importantly, *cannot* remove all structural defects (and oxygen containing groups[9]) introduced during the oxidation process[10,11] Therefore, both GO and r-GO remain significantly inferior to graphene in terms of structure and physicochemical properties as recently highlighted in the literature.[12-14] In this context the development of single and/or few layered graphene sheets through controlled liquid-phase exfoliation of graphite plays a pivotal role[15-17] as a direct, facile, and benign production of graphene avoiding the oxidation step.[4] Graphene produced in this way forms rather stable, colloidal dispersions in certain solvents, thereby enabling further manipulation of the sheets in various processes (*e.g.* blending, impregnation, spin-coating) or chemical functionalization via chemical reactions already well-established for other forms of carbon nano-structured materials (*e.g.* carbon nanotubes) such as the chemical functionalization via 1,3-dipolar cycloaddition.[18-20]

Metal nanoparticles (denoted hereafter as NPs) have emerged as a new class of compounds that are particularly interesting for their unique electronic, optical, magnetic and catalytic properties.[21,22] Iron oxide NPs in particular, hold a special place within this family, not only because iron is the fourth most plentiful element in the earth's crust but also because Fe has the highest room-temperature value of the spontaneous magnetization, σs, of any known element, and exhibits a low magnetocrystalline anisotropy as well as an attractive Curie temperature.[23] Iron oxide NPs have received particular attention because in addition to their unique magnetic properties,[24-26] they are also very attractive candidates for applications in diverse fields, including biomedicine[27-30] and catalysis.[31-35]

Literature reports on *in-situ* growth of *iron oxide* nanoparticles towards the synthesis of NPs/graphene-based hybrids involve the use of either GO[36-39] or r-GO,[40-43] with the drawbacks discussed above. Alternative protocols for the production of iron oxide NPs-graphene hybrids, based on the liquid-phase exfoliation of graphite are scarce[44,45] and most

importantly focus on the separate synthesis of functionalized graphene and *pre-formed* NPs, which are then connected in a complicated procedure requiring additional experimental synthetic efforts (*i.e.* suitable surface functionalization of NPs to match the surface chemical groups of graphene, wet chemistry processes to connect pre-formed NPs and functionalized graphene *etc*.) and chemical reagents/organic solvents.

Here instead, we report the synthesis of iron oxide NP-graphene magnetic hybrid materials employing high-quality, single and/or very few layered graphene sheets produced from the liquid-phase exfoliation of graphite and the subsequent *in-situ* synthesis of uncapped NPs at the graphene's surface. Our approach does not include any oxidation treatment of the source material (graphite), with beneficial consequences to the physicochemical properties of the resulting graphene sheets. In addition, it does not require the separate synthesis of *pre-formed* metal NPs, as well as the extra synthetic step required to connect *pre-formed* metal NPs with exfoliated graphene. Moreover, the proposed strategy yields capping-free NPs which exhibit a fully accessible surface (an important prerequisite in diverse fields like catalysis,[46,47] bio-sensors[48,49] and energy-related applications[50]). Therefore, there is no need for further treatment in order to eliminate the employed surfactants and/or capping agents (which is the case for *pre-formed* NPs).

2. Results and Discussion

A schematic overview of the synthetic approach employed for the preparation of the hybrid materials is presented in Fig. 1. Graphene sheets produced from the liquid-phase exfoliation of graphite were chemically functionalized via well-established chemical routes based on 1, 3-dipolar cycloaddition reactions (Fig. 1a).[18] The introduced chemical groups were then used as "anchor-sites" for the selected immobilization of the NP precursor (Fe cations) (Fig. 1b). Next, acetic acid fumes were brought to interact with the graphene/precursor solid mixture to further stabilize the Fe cations prior to NP growth.[24,51] Subsequently, iron oxide NPs were grown *in-situ* (via thermal treatment) on the graphene sheets yielding the final hybrid materials (denoted hereafter as *NPs@Graph*, Fig 1c).

TEM analysis, shown in Fig. 2, confirmed the presence of iron oxide NPs on the surface of the exfoliated graphene sheets. The images documented the development of rather uniform and relatively small in size and round in shape NPs finely dispersed over the graphene surfaces (Fig 2a, b). Although the density of NPs appeared to be quite high, no significant accumulation or aggregation into larger assemblies was observed. Based on a statistical analysis of the acquired TEM images, the average size of the synthesized NPs was estimated to be about 10(±2) nm (see histogram Sup. Info. S1-top) in agreement with the

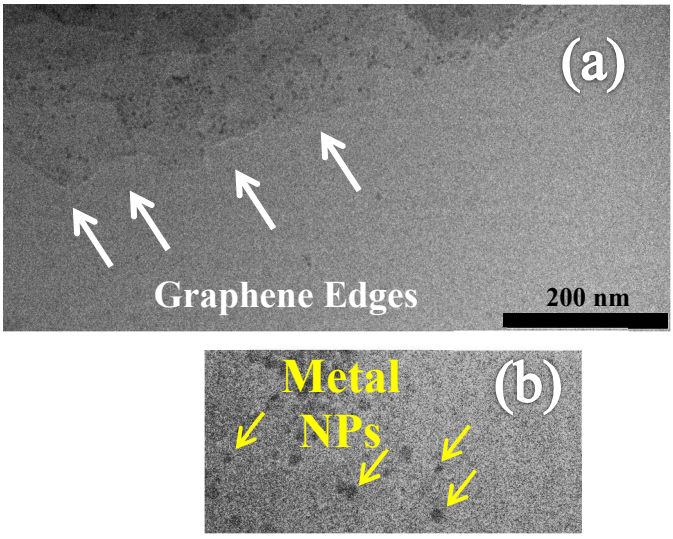

Fig. 2. TEM images of synthesized NPs@Graph hybrids

average particle size calculated from the corresponding XRD pattern using the Scherrer formula (discussed below). Furthermore, the TEM analysis revealed the presence of transparent and crystalline very thin sheets (Fig. 2a), providing a first indication of the stacking configuration of graphene sheets in the final hybrids; no multi-layered structures as found for graphite crystallites were noticed. The EDX spectrum of the *NPs@Graph* hybrids (Sup. Info. S1-bottom) showed nitrogen and carbon signals originating from the functionalized graphene. In addition, the spectrum testified the presence of iron and oxygen attributed to the iron oxide NPs; neither iron nor oxygen were recorded in the corresponding EDX spectrum of functionalized graphene.

The successful formation of NPs was further confirmed by atomic force microscopy (AFM). In agreement with the TEM analysis discussed above, the AFM images of *NPs@Graph* hybrids (Fig. 3) showed the successful growth of relative small and uniform NPs on the graphene surface. The analysis of the height profile (Fig. 3a), showed that the mean, average size of the NPs deposited on the graphene sheets was about 10(±2) nm, the same value obtained from TEM analysis. Furthermore, detailed height profile measurements by AFM at the edges of the graphene sheets in *NPs@Graph* (Fig 3b) showed a height of less than 2 nm, a value typically reported for single or few layer graphene sheets[52] and corresponding (in our case) to approximately 5-6 sheets. This finding was further confirmed by Raman results as discussed further down. This indicates that

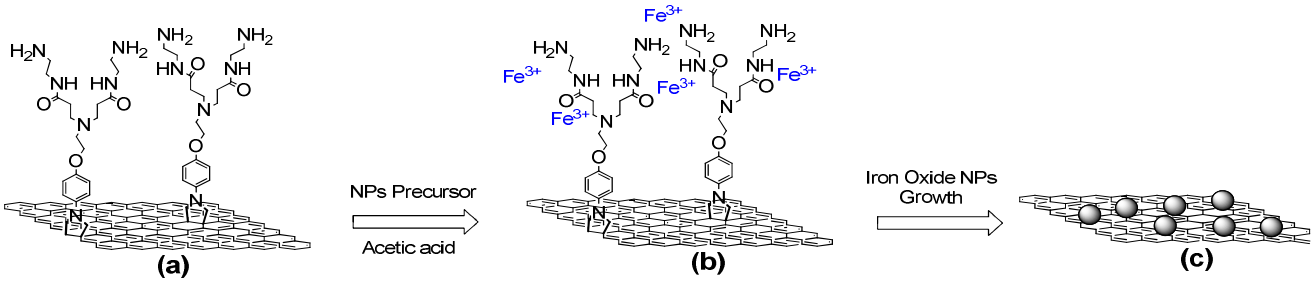

Fig. 1. A schematic representation of the synthetic approach.

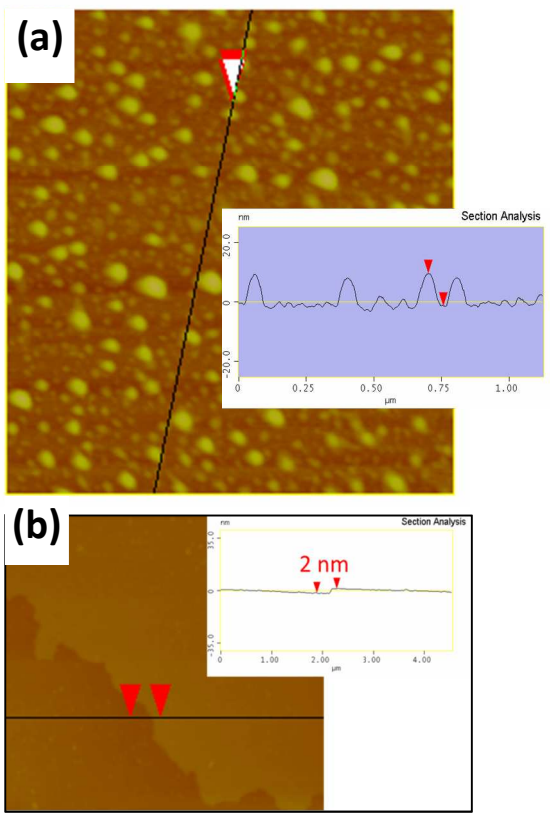

Fig. 3. AFM images and corresponding cross-section profiles of NPs (a) and graphene sheets (b) in the synthesized *NPs@Graph* hybrids.

during the growth of NPs the single graphene sheets retained their exfoliated configuration to a large extent; no significant restacking leading to a multi-layer configuration was observed. This conclusion is further supported by Raman studies discussed below.

To retrieve information regarding the crystalline phases present in the *NPs@Graph* hybrids XRD measurements were performed. The XRD pattern (Fig. 4a) exhibited a set of relatively broad Bragg reflections attributed to the formation of a spinel-type iron oxide nanocrystalline phase. The peaks' large broadening resulting from the NPs' small size did not allow us to safely distinguish the different crystalline phases from the observed reflections in a particular pattern, since both maghemite γ-Fe_2O_3 and magnetite Fe_3O_4 exhibit very similar X-ray diffractograms.[53]

The Scherrer equation[54] allows estimating the average size of the synthesized NPs as about 10±2 nm. Another interesting finding is the absence of any strong diffraction peak at around $2\theta=26^o$. This 2θ value corresponds to the characteristic 002 graphitic peak, reported for graphite,[55] multi-walled carbon nanotubes[56] and similar multi-layered graphitic structures.[57] This observation again suggests that the graphene sheets in the final hybrids did not restack to form multilayer structures, in agreement with the findings of the AFM and TEM analysis.

To gain insight into the elemental composition and the chemical state of the elements composing the intermediate and

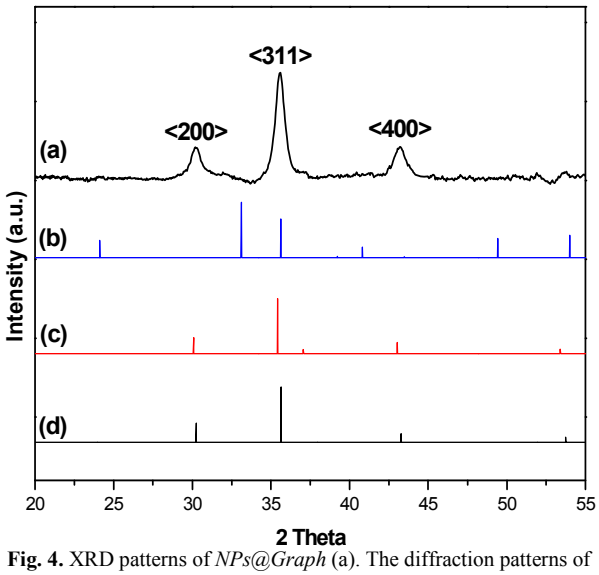

Fig. 4. XRD patterns of *NPs@Graph* (a). The diffraction patterns of α-Fe_2O_3 (b, JCPDS 46-1312), Fe_3O_4 (c, JCPDS 19-629) and γ-Fe_2O_3 (d, JCPDS 39-1346) are also shown for comparison.

final materials, XPS spectra of functionalized graphene, of functionalized graphene after interacting with acetic acid and the NP precursor, as well as of the *NPs@Graph* hybrid were collected. The spectral analysis procedure consisted of mathematically reconstructing each spectrum with a minimum number of peaks consistent with the raw data and the molecular structure. Three contributions to the carbon 1*s* core level region of the XPS spectrum recorded on functionalized graphene can be identified (Fig. 5a), namely a component at a binding energy of 284.6 eV, attributed to C-C bonds of the hexagonal lattice, which accounts for 60 % of the overall carbon intensity; a second contribution at 285.8 eV, due to C-N and C-O bonds (30% of the total carbon intensity), and a third component at 287.0 eV assigned to carbonyl groups (C=O, 10 % of the overall carbon intensity). These XPS data therefore confirm the successful functionalization of graphene. The C 1*s* core level region of the XPS spectrum of functionalized graphene after interaction with the NP precursor and acetic acid (shown in Fig. 5b), exhibits an additional fourth component at a binding energy of 288.7 eV, which is attributed to carboxylic (-COOH) groups and accounts for 17% of the overall carbon intensity. These groups originate from the successful adsorption of the acetic acid, used for the stabilization of the NP precursor. Additional evidence towards the same conclusion comes from the comparison of the N 1*s* core level region of the XPS spectra of functionalized graphene before and after interacting with the Fe precursor and acetic acid shown in Fig.6. Before the immobilization of Fe cations the spectrum (Fig. 6a) can be fitted with two peaks, namely a contribution at 399.6 eV, attributed to pyrrolidine-like nitrogen atoms, and the contribution due to the positively charged protonated amino groups (NH^{3+}) at a binding energy of 401.1 eV, both introduced after the organic functionalization of liquid-phase exfoliated graphene as we previously reported.[18] The profile of the N 1*s* spectrum after the interaction with Fe cations and acetic acid

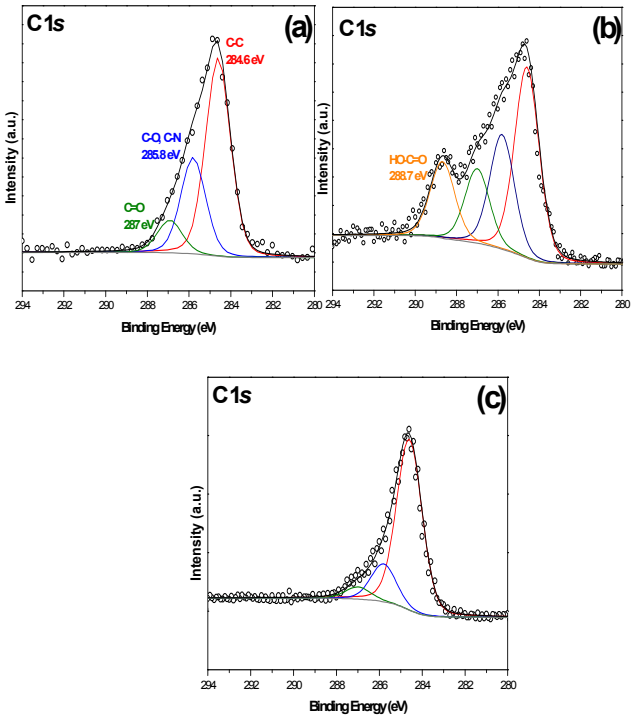

Fig. 5. The C 1*s* core level region of the XPS spectra of functionalized graphene (a), functionalized graphene after interacting with acetic acid and NP precursor (b) and *NPs@Graph* hybrids (c). Experimental data (o) and fit (-).

shows the same profile (Fig. 6b) with the exception of a shift in binding energy. In particular, the pyrrolidine-like nitrogen appeared at 399.3 eV, while the amine-related contribution was

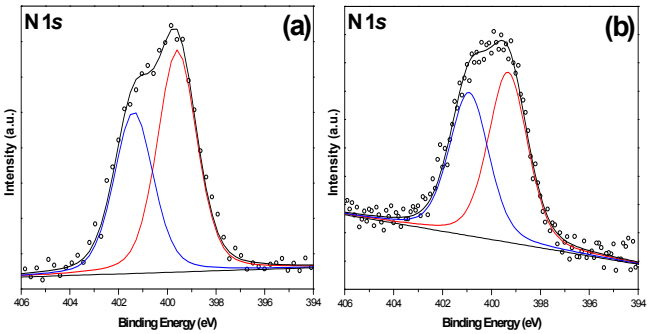

Fig. 6. The N 1*s* core level region of the XPS spectra of functionalized graphene (a) and functionalized graphene after interacting with acetic acid and NP precursor (b). Experimental data (o) and fit (-).

recorded at 400.8 eV. Nevertheless, the relative intensity of the two components was not changed compared to the spectrum of starting functionalized graphene material. The shift in binding energy suggests the successful adsorption of Fe cations and acetic acid in agreement with the findings derived from analysis of C 1*s* region. Further proof was provided by the analysis of the C 1*s* spectrum of the *NPs@Graph* hybrids (Fig. 5c). The C 1*s* spectrum of *NPs@Graph* was fitted using three contributions. The major contribution at 284.6 eV (accounting for 77 % of overall C 1*s* intensity) derives from C-C bonds, the second contribution at 285.8 eV (17% of the total C 1*s*

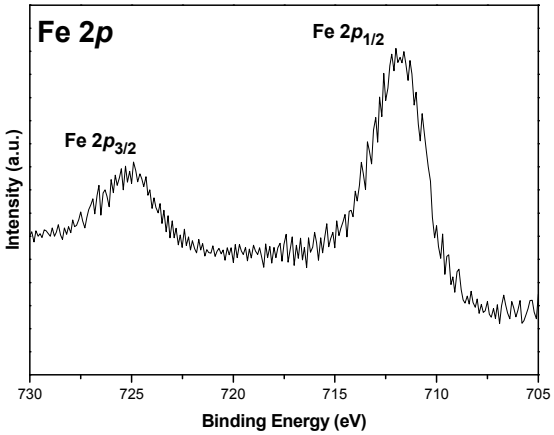

Fig. 7. The Fe 2*p* core level region of the XPS spectrum of the *NPs@Graph* hybrid.

intensity) is due to C-O and C-N bonds and the last one at 287.0 eV (6% of the overall C 1*s* intensity) is assigned to C=O bonds. The fourth contribution due to adsorbed acetic acid (Fig. 5b) was not present in the spectrum of the final hybrids, testifying to the removal of acetic acid during the prolonged heating at elevated temperature that took place during NPs growth. The lower relative intensities of C-O and/or C-N, and C=O contributions as compared to the corresponding values for the functionalized graphene starting material (Fig. 5a) can also be explained as due to the heating. A similar behaviour involving the partial removal of nitrogen- and/or oxygen-containing groups is commonly reported in XPS studies of carbon-based nano-structured materials (including graphene) after controlled heating at similar temperatures.[58,59]

The Fe 2*p* region of the XPS spectrum of *NPs@Graph* (Fig. 7) exhibits the Fe $2p_{3/2}$ and Fe $2p_{1/2}$ contributions at 711.6 and 725 eV, respectively. The profile of the spectrum resembles published spectra of Fe_3O_4.[44,60] This, together with the absence of the charge transfer satellite of Fe $2p_{3/2}$ at 720 eV characteristic for γ-Fe_2O_3[61] points to the conclusion that magnetite is the dominant phase in the synthesized NPs.

Raman spectroscopy was also employed to study the intermediate products (exfoliated graphene sheets, functionalized graphene sheets) and the final product of the synthesis (*NPs@Graph* hybrid material), as illustrated in Fig. 8. The spectrum of the starting graphene sheets produced from the liquid-phase exfoliation (Fig. 8a) showed two major Raman features; the vibrational G band and the two-phonon 2D band. The position and shape of the 2D band at about 2700 cm^{-1} as well as the intensity ratio between the G and the 2D band strongly suggest the presence of few-layer graphene aggregates in agreement with previous reports.[62] After functionalization the product showed a high-intensity D band at about 1350 cm^{-1} (Fig. 8b) which is commonly attributed to the presence of defects in the lattice well as to the result of the occurred organic functionalization.[18] The Raman spectrum of *NPs@Graph* shows the same profile but the intensity of the D-band is further increased (Fig. 8c). This additional increase of the D band intensity in the final hybrids is attributed to an even higher

defect density that was introduced during the thermal treatment of graphene to induce the growth of iron oxide NPs. Nevertheless, graphene sheets retained their overall structural quality in the final hybrids as suggested by the observed relative D to G band and G to 2D band intensity ratios.

Thermal analysis measurements (TGA) provided additional quantitative information about the synthesized *NPs@Graph* hybrid material. The TGA diagram (recorded under air flow) of

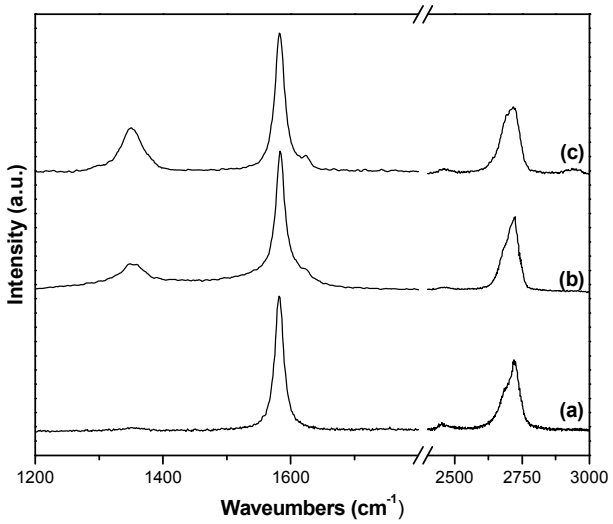

Fig. 8. Raman spectra of liquid-phase exfoliated graphene sheets (a), chemically functionalized graphene sheets (b), and the final *NPs@Graph* hybrid (c).

the chemically functionalized graphene is presented in Fig. 9a. The weight loss (about 30% of the initial overall weight) in the temperature range 100-350 °C is attributed to the thermal removal of the organic groups introduced during the chemical functionalization. Above 415 °C, the sharp weight loss indicates the thermal destruction of the graphitic network. On the contrary, the TGA diagram of *NPs@Graph* (also recorded under air flow, Fig. 9b) did not show any significant weight loss in the temperature range 100-350 °C, since the introduced organic groups were already removed during the thermal treatment to induce NP growth. Most importantly, the recorded weight loss above 450 °C is only 70% of the initial weight. The remaining 30% weight can be assumed to correspond to the synthesized magnetite-rich NPs since at this temperature the graphene portion present in the final hybrids was selectively removed during the heating ramp of the TGA measurement.

The magnetic behaviour of the synthesized *NPs@Graph* hybrids, was investigated in detail as a function of applied field and temperature. Specifically, Fig. 10-Left presents the zero field cooling (ZFC) and field cooling (FC) magnetization curves of the *NPs@Graph* in the temperature range 5-300 K. Samples were cooled down to 5 K without a magnetic field and then a field of 500 Oe was applied to record the ZFC magnetization as a function of temperature from 5-300 K. For the FC, samples were cooled down from room temperature to 5 K in a magnetic field of 500 Oe and then measurements were taken in the temperature range 5-300 K. The ZFC and the FC data show a divergence at around 270 K. The ZFC curve

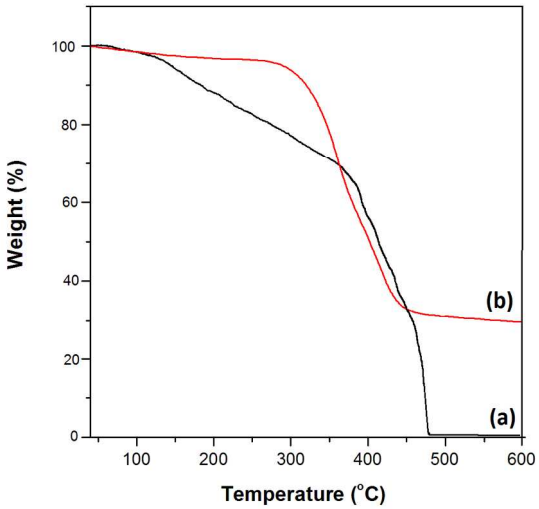

Fig. 9. TGA measurements of the chemically functionalized graphene sheets (a) and the final *NPs@Graph* hybrid (b).

exhibits a broad peak, the maximum of which (TP) is influenced by various factors such as inter-particle distance, size and shape distribution of particles. Despite of various influencing factors for TP, this temperature is roughly identified as the average blocking temperature of the material. This type of ZFC and FC behaviour has also been seen for other magnetite nanoparticles based hybrid materials.[63] A rather broad and flat plateau for the ZFC cure could be understood in the context of particles with varying size and inter-particle distance.[63]

Magnetization vs field (M-H) curves at different temperatures of the *NPs@Graph* are shown in Fig. 10-Right. The room temperature hysteresis shows a coercive field of 50 Oe that increases up to 507 Oe at 5 K. A very small coercive field in the former case is typical of superparamagnetism, which is manifest in *NPs@Graph* because the particle size is smaller than a single domain (~54 nm).[64] Fig. 10-Right also shows a very small saturation magnetization in *NPs@Graph* as compared to bulk magnetite (92 emu/g). This has also been observed in previous reports where it has been attributed to the small size of the nanoparticles, and pinning of the surface spins.[65-67]

The synthesized *NPs@Graph* hybrids could be dispersed in aqueous solutions (up to a concentration of 0.6 mg/ml), and the derived dispersions were stable for several days without any noticeable sings of precipitation. Very interestingly, and due to their magnetic properties the solids could be easily re-collected and isolated with the aid of a magnet (Sup. Info. S3). The latter clearly highlights the efficient and sustainable use and recovery of the developed hybrids in applications requiring their dispersion in liquid media (e.g. catalysis of aqueous pollutants, drug delivery etc)".

Using our proposed synthetic methodology, we also investigated the effect of employing different initial mass ratio of graphene:NP precursor on the morphology of the resulting

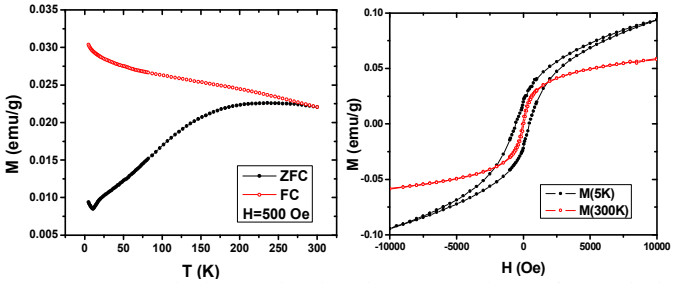

Fig. 10. Magnetization as a function of temperature for *NPs@Graph* in the ZFC and FC modes at the applied magnetic field (H) of 500 Oe (*left*) and M-H curves for NPs@Graph at T = 300 K and 5 K (*right*).

hybrids and explore whether the size and/or population of attached NPs at graphene be modified. However when the initial mass ratio of graphene-NP precursor was increased to 1:2, the resulting hybrids were mainly composed of large, aggregated NPs assemblies (Sup. Info. S2) rather than isolated, small, homogeneously distributed NPs. We also investigated a lower (1:0.5) initial mass ratio but found only a very small number of NPs attached to the Graphene surface in this case and consequently a poor magnetic behaviour of the hybrid. The 1:1 mass ratio is therefore the optimal one.

3. Conclusions

In conclusion, we demonstrated the successful development of magnetite-rich, very small in size (<12nm), spherical NPs on the surface of graphene sheets produced via the liquid-phase exfoliation of graphite. TEM, XRD and AFM results indicate that the graphene sheets in the final hybrids did not restack into multi-layered structures, while Raman spectroscopy confirmed their good structural quality. Additional Raman measurements in conjunction with XPS studies shed light on the various intermediate products of the adopted synthetic steps. A quantification of the NPs yield was derived from TGA data, suggesting a content of magnetite-rich NPs up to 30% wt. in final hybrids. Magnetic measurements showed room temperature superparamagnetism in the hybrid material. Our reported synthetic approach opens new perspectives for the development of graphene-based hybrid materials useful in applications related to magnetism, catalysis and biomedicine. Especially with regards to the latter two applications, this route is particularly attractive due to the complete absence of any coupling agent and/or surfactant on the surface of synthesized NPs, which makes these NPs fully accessible for catalytic and bio-related processes.

4. Experimental

Liquid-phase exfoliation of graphene: Graphite (Bay Carbon, Inc., SP-1 graphite powder). Graphite was exfoliated according to previously reported, well-established and widely accepted routes.[18-20]

Chemical functionalization of graphene (Sup. Info. S4): Fifty mL of exfoliated graphite solution was used to carry out the reaction. The graphene concentration of the solution was calculated by the optical characterization reported by Coleman and co-workers.[68] The concentration was found to range from 0.01 ± 0.005 mg/mL. To perform the organic reaction, 1.5 equiv. with respect to graphene of N-(hydroxyphenyl)-glycine and paraformaldehyde was added to the graphene suspension. The reaction mixture was heated at 125 °C under magnetic stirring, while the reagents were added each 24 h for 3 days. The resulting mixture was filtered with a Millipore system (JH 0.45 um filter), and the solid was washed thoroughly with methanol until the solvent was clear. The product was dispersed in 20 mL of DMF by mild sonication. The functionalized graphene solution reacted with the Dendron structure 2 (Sup. Info. S5) in an excess of 10% with the equimolar addition of K_2CO_3, followed by heating at 100 °C for 3 days. Subsequently the mixture was filtered and washed thoroughly with the use of DMF, MeOH and THF. The collected powder was re-dispersed in MeOH and allowed to further react with excess of ethylene diamine at 60 °C for 3 days. The final material was filtered and washed with distilled water, MeOH and THF. TGA analysis confirmed the successful attachment of the dendron structure (Sup. Info. S6). The quantification of the free amino groups present on dendrons was carried out by the quantitative Kaiser test. Graphene resulted in average as 0.584 mmol/g of amino groups.

Development of iron oxide nanoparticles on graphene: The iron oxide NP/graphene hybrids were prepared based on a modified wet impregnation method previously reported.[24,51] A certain quantity of chemically functionalized graphene was dispersed in 50 ml of CH_3OH containing an quantity of $Fe(NO_3)_3{\cdot}9H_2O$ (100 mg, Aldrich) to produce samples with a Graphene: $Fe(NO_3)_3{\cdot}9H_2O$ weight ratio of 1:1. The mixture was further stirred for 6 h, followed by rapid removal of the solvent at 70 °C. The as-prepared powder was exposed to vapours of acetic acid (99.5% Aldrich) at 70 °C for 1 h. The obtained sample was further dried for 15 min at 70 °C in order to remove any physically absorbed acetic acid. The final *NPs@Graph* hybrid material was obtained by calcination for 1 h at 400 °C under high-purity argon flow (50 sccm, 99.999%).

Characterization:

Powder X-ray Diffraction (XRD). The XRD patterns were collected with a Philips PANanlytical X'Pert MRD diffractometer with a Cu Kα radiation (λ = 1.5418 Å) using an anode voltage of 40 kV and a current of 40 mA, a 0.25° divergent slit and a 0.125° anti-scattering slit. The patterns were recorded in a 2θ range from 1° to 10°, in steps of 0.01° with a counting time of 15 s each. Samples were in the form of films supported on SiO_x substrates.

Raman: Raman spectra were recorded with a Micro–Raman system RM 1000 (RENISHAW) using a laser excitation line at 532 nm (Nd–YAG) in the range of 1.000–2.800 cm-1. A power of 1 mW was used with 1 μm focus spot in order to avoid photodecomposition of the samples.

X-ray Photoelectron Spectroscopy (XPS): For the XPS measurements, evaporated gold films supported on mica were used as substrates. Each sample was dispersed in ethanol, and after short stirring for 30 min, a small drop of the suspension was deposited on the Au substrate and left to dry in air.[69] Samples were introduced via a load lock system into a SSX-100 (Surface Science Instruments) photoelectron spectrometer equipped with a monochromatic Al Kα X-ray source (hν = 1486.6 eV). The base pressure in the spectrometer was 1×10^{-10} Torr during all measurements. The energy resolution was set to 1.3 eV to minimize measuring time. The photoelectron take-off angle was 37°. An electron flood gun providing 0.3 eV kinetic energy electrons in combination with an Au grid placed 1 mm above the sample was used to compensate for sample charging. Spectral analysis included a Shirley background subtraction and peak deconvolution employing mixed Gaussian−Lorentzian functions, in a least squares curve-fitting program (WinSpec)

developed at the LISE, University of Namur, Belgium. Binding energies were referenced to the C 1*s* photoemission peak of aromatic carbon, centred at 285 eV,[38] and are reported ±0.1 eV.

Thermogravimetric measurements (TGA): TGA measurements were recorded using either a Thermo Scientific thermogravimetric analyzer. Samples of approximately 5 mg were heated under air flow from 40 to 800 °C at a rate of 5 °C/min or (in the case of functionalized graphene derivatives) a TGA Q500 (TA instrument), under N_2, by equilibrating at 100 °C, and following a ramp at 10°C/min up to 1000 °C.

Atomic Force Microscopy: AFM images were obtained in tapping mode with a Multimode Nanoscope 3D using Tap-300G silicon cantilevers with a tip radius <10 nm and a force constant of ≈20–75 N m^{-1}. Samples were deposited onto silicon wafers (P/Bor, single side polished) from dilute aqueous dispersions by drop casting.

Transmission Electron Microscopy: TEM analysis was performed with a Philips CM12 microscope operating at 120 kV, on samples prepared by drop casting onto formvar/carbon copper grids (200 mesh). To prepare the suspension for drop-casting, the samples were sonicated in EtOH for 2 minutes using a Julabo USR3 Labortechnic bath sonicator (35 kHz, Power 2 x 150W) while cooling with a water/ice mixture. TEM images were recorded with a CCD camera (Gatan 791).

Magnetic measurements: The magnetic behaviour of the sample was studied using a SQUID based magnetic property measurement system (Model: MPMS-Quantum Design7).

Acknowledgements

This work was performed within "Top Research School" program of the Zernike Institute for Advanced Materials under the Bonus Incentive Scheme (BIS) of the Netherlands' Ministry of Education, Science, and Culture and received additional support from the "Graphene-based Electronics" research program of the Foundation for Fundamental Research on Matter (FOM)', which is financially supported by the Netherlands Organisation for Scientific Research (NWO). Additional, partially support was provided by EU under the FP7 PEOPLE-2012-IAPP-SANAD (No 324443) project. This work was supported by the University of Trieste, Consorzio Interuniversitario Nazionale per la Scienza e Tecnologia dei Materiali (INSTM), Ministero dell'Università e della Ricerca (MIUR) (FIRB prot. RBAP11ETKA and Cofin. Prot. 2010N3T9M4).

Notes and References

[a] Zernike Institute for Advanced Materials, University of Groningen, Nijenborgh 4, NL-9747AG Groningen, the Netherlands.

[b] Center of Excellence for Nanostructured Materials (CENMAT) and INSTM, unit of Trieste, Department of Chemical and Pharmaceutical Sciences, University of Trieste, via L. Giorgieri 1, 34127 Trieste, Italy.

[c] Institute of Nanoscience & Nanotechnology, National Center for Scientific Research "Demokritos", GR-15310, Athens, Greece.

[d] Department of Materials Science and Engineering, University of Ioannina, GR-45110 Ioannina, Greece.

1. K. S. Novoselov, A. K. Geim, S. V. Morozov, D. Jiang, Y. Zhang, S. V. Dubonos, I. V. Grigorieva and A. A. Firsov, *Science*, 2004, **306**, 666.
2. K. Spyrou, D. Gournis and P. Rudolf, *ECS J. Solid State Sci. Tec.*, 2013, **2**, M3160.
3. W. S. Hummers and R. E. Offeman, *J. Am. Chem. Soc.*, 1958, 80, 1339.
4. B. C. Brodie, *Annalytic Chimie Physics*, 1860, **59**, 466
5. D. R. Dreyer, S. Park, C. W. Bielawski and R. S. Ruoff, *Chem. Soc. Rev.*, 2010, **39**, 228.
6. N. Tombros, C. Jozsa, M. Popinciuc, H. T. Jonkman and B. J. Van Wees, *Nature*, 2007, **448**, 571.
7. X. Du, I. Skachko, A. Barker and E. Y. Andrei, *Nature Nanotechnology*, 2008, **3**, 491.
8 I. Jung, M. Pelton, R. Piner, D. A. Dikin, S. Stankovich, S. Watcharotone, M. Hausner and R. S. Ruoff, *Nano Lett.*, 2007, **7**, 3569.
9. D. W. Boukhvalov and M. I. Katsnelson, *J. Am. Chem. Soc.*, 2008, **130**, 10697.
10. D. Yang, A. Velamakanni, G. Bozoklu, S. Park, M. Stoller, R. D. Piner, S. Stankovich, I. Jung, D. A. Field, C. A. Ventrice Jr and R. S. Ruoff, *Carbon*, 2009, **47**, 145.
11. H. Kang, A. Kulkarni, S. Stankovich, R. S. Ruoff and S. Baik, *Carbon*, 2009, **47**, 1520.
12. A. Ciesielski and P. Samori, *Chem. Soc. Rev.*, 2014, **43**, 381.
13. G. H. Nam, S. H. Baek, C. H. Cho and I. K. Park, *Nanoscale*, 2014, **6**, 11653.
14. Y. Song, D. Y. Feng, T. Y. Liu, Y. Li and X. X. Liu, *Nanoscale*, 2015, **7**, 3581.
15. Y. Hernandez, V. Nicolosi, M. Lotya, F. M. Blighe, Z. Sun, S. De, I. T. McGovern, B. Holland, M. Byrne, Y. K. Gun'Ko, J. J. Boland, P. Niraj, G. Duesberg, S. Krishnamurthy, R. Goodhue, J. Hutchison, V. Scardaci, A. C. Ferrari and J. N. Coleman, *Nat. Nanotech*, 2008, **3**, 563.
16. A. B. Bourlinos, V. Georgakilas, R. Zboril, T. A. Steriotis and A. K. Stubos, *Small*, 2009, 5, 1841.
17. M. Lotya, Y. Hernandez, P. J. King, R. J. Smith, V. Nicolosi, L. S. Karlsson, F. M. Blighe, S. De, W. Zhiming, I. T. McGovern, G. S. Duesberg and J. N. Coleman, *J. Am. Chem. Soc*., 2009, **131**, 3611.
18. M. Quintana, K. Spyrou, M. Grzelczak, W. R. Browne, P. Rudolf and M. Prato, *ACS Nano*, 2010, **4**, 3527.
19. M. Quintana, A. Montellano, A. E. Del Rio Castillo, G. V. Tendeloo, C. Bittencourt and M. Prato, *Chem. Commun.*, 2011, **47**, 9330-9332.
20. M. Quintana, E. Vazquez and M. Prato, *Accounts Chem. Res.*, 2013, **46**, 138.
21. G. Schmid, ed., Nanoparticles, Wiley-VCH, Weinheim, 2004.
22. V. Rotello, ed., Nanoparticles: Building Blocks for Nanotechnology, Kluver Academic/Plenum Publishers, New York, 2004.
23. D. L. Huber, *Small*, 2005, **1**, 482.
24. T. Tsoufis, A. P. Douvalis, C. E. Lekka, P. N. Trikalitis, T. Bakas and D. Gournis, *J. Nanopart. Res.*, 2013, **15,** 1924
25. B. Chertok, B. A. Moffat, A. E. David, F. Yu, C. Bergemann, B. D. Ross and V. C. Yang, *Biomaterials*, 2008, **29**, 487
26. L. A. Harris, J. D. Goff, A. Y. Carmichael, J. S. Riffle, J. J. Harburn, T. G. St. Pierre and M. Saunders, *Chem. Mat.*, 2003, **15**, 1367.
27. A. K. Gupta and M. Gupta, *Biomaterials*, 2005, **26**, 3995.
28. M. Liong, J. Lu, M. Kovochich, T. Xia, S. G. Ruehm, A. E. Nel, F. Tamanoi and J. I. Zink, *ACS Nano*, 2008, **2**, 889.
29. A. K. Gupta, R. R. Naregalkar, V. D. Vaidya and M. Gupta, *Nanomedicine-UK*, 2007, **2**, 23.

30. C. C. Berry and A. S. G. Curtis, *J. Phys. D: Appl. Phys.*, 2003, **36**, R198.
31. H.-H. Yang, S.-Q. Zhang, X.-L. Chen, Z.-X. Zhuang, J.-G. Xu and X.-R. Wang, *Anal. Chem.*, 2004, **76**, 1316.
32. H. Wei and E. Wang, *Anal. Chem.*, 2008, **80**, 2250.
33. P. Li, D. E. Miser, S. Rabiei, R. T. Yadav and M. R. Hajaligol, *Appl. Catal. B - Environ.*, 2003, **43**, 151.
34. F. Shi, M. K. Tse, M. M. Pohl, A. Brückner, S. Zhang and M. Beller, *Angew. Chem. Int. Edit.*, 2007, **46**, 8866.
35. J. M. Perez, *Nat. Nanotec.*, 2007, **2**, 535.
36. H. Li, Q. Zhao, X. Li, Z. Zhu, M. Tade and S. Liu, *J. Nanopart. Res.*, 2013, **15**, 1423.
37. Y. Xue, H. Chen, D. Yu, S. Wang, M. Yardeni, Q. Dai, M. Guo, Y. Liu, F. Lu, J. Qu and L. Dai, *Chem. Commun.*, 2011, **47**, 11689.
38. L. Ai, C. Zhang and Z. Chen, *J. Hazard. Mater.*, 2011, **192**, 1515.
39. H. He and C. Gao, *ACS Appl. Mater Interf.*, 2010, **2**, 3201.
40. T.V. Thu, A. Sandhu, *Mater. Sci. Eng. B,* 2014, **13**, 189.
41. X. Zhu, Y. Zhu, S. Murali, M. D. Stoller and R. S. Ruoff, *ACS Nano*, 2011, **5**, 3333.
42. Y. Liang, Y. Li, H. Wang, J. Zhou, J. Wang, T. Regier and H. Dai, *Nat. Mater.*, 2011, **10**, 780.
43. H. Wang, L. F. Cui, Y. Yang, H. Sanchez Casalongue, J. T. Robinson, Y. Liang, Y. Cui and H. Dai, *J. Am. Chem. Soc.,* 2010, **132**, 13978.
44. V. Papaefthimiou, I. Florea, W. Baaziz, I. Janowska, W. H. Doh, D. Begin, R. Blume, A. Knop-Gericke, O. Ersen, C. Pham-Huu and S. Zafeiratos, *J. Phys. Chem. C*, 2013, **117**, 20313.
45. D. Ihiawakrim, O. Ersen, F. Melin, P. Hellwig, I. Janowska, D. Begin, W. Baaziz, S. Begin-Colin, C. Pham-Huu and R. Baati, *Nanoscale*, 2013, **5**, 9073.
46. Y. Liang, Y. Li, H. Wang, J. Zhou, J. Wang, T. Regier and H. Dai, *Nat. Mater.*, 2011, **10**, 780.
47. S. Guo and S. Sun, *J. Am. Chem. Soc.,* 2012, **134**, 2492.
48. S. Guo and E. Wang, *Nano Today*, 2011, **6**, 240.
49. T. Kuila, S. Bose, P. Khanra, A. K. Mishra, N. H. Kim and J. H. Lee, *Biosens. Bioelectron.*, 2011, **26**, 4637.
50. P. V. Kamat, *J. Phys. Chem. Lett.*, 2010, **1**, 520.
51. M. A. Karakassides, D. Gournis, A. B. Bourlinos, P. N. Trikalitis and T. Bakas, *J. Mater. Chem.*, 2003, **13**, 871.
52. V. Georgakilas, A. B. Bourlinos, R. Zboril, T. A. Steriotis, P. Dallas, A. K. Stubos and C. Trapalis, *Chem. Commun.,* 2010, **46**, 1766.
53. R. M. Cornell and U. Schwertmann, The Iron Oxides: Structure, Properties, Reactions, Occurrences and Uses, Wiley-VCH, Weinheim, 2003.
54. B. D. Cullity, Elements of X-ray Diffraction, Addison-Wesley, Reading, Massachusetts, 1956.
55. K. S. Subrahmanyam, S. R. C. Vivekchand, A. Govindaraj and C. N. R. Rao, *J. Mater. Chem.*, 2008, **18**, 1517.
56. K. Kardimi, T. Tsoufis, A. Tomou, B. J. Kooi, M. I. Prodromidis and D. Gournis, *Int. J. Hydrogen Ener.*, 2012, **37**, 1243.
57. E. S. Steigerwalt, G. A. Deluga, D. E. Cliffel and C. M. Lukehart, *J. Phys. Chem. B*, 2001, **105**, 8097.
58. S. Kundu, Y. Wang, W. Xia and M. Muhler, *J. Phys. Chem. C*, 2008, **112**, 16869.
59. S. H. Tamboli, B. S. Kim, G. Choi, H. Lee, D. Lee, U. M. Patil, J. Lim, S. B. Kulkarni, S. C. Jun and H. H. Cho, *J Mater. Chem. A*, 2014, **2**, 5077.
60. M. Descostes, F. Mercier, N. Thromat, C. Beaucaire and M. Gautier-Soyer, *Appl. Surf. Sci.,* 2000, **165**, 288.
61. A.-L. Morel, S. I. Nikitenko, K. Gionnet, A. Wattiaux, J. Lai-Kee-Him, C. Labrugere, B. Chevalier, G. Deleris, C. Petibois, A. Brisson and M. Simonoff, *ACS Nano*, 2008, **2**, 847.
62. A. C. Ferrari, J. C. Meyer, V. Scardaci, C. Casiraghi, M. Lazzeri, F. Mauri, S. Piscanec, D. Jiang, K. S. Novoselov, S. Roth and A. K. Geim, *Phys. Rev. Lett.*, 2006, **97**, 187401.
63. V. N. Nikiforov, Y. A. Koksharov, S. N. Polyakov, A. P. Malakho, A. V. Volkov, M. A. Moskvina, G. B. Khomutov and V. Y. Irkhin, *J. Alloys Compd.,* 2013, **569**, 58.
64. A. Aharoni and J. P. Jakubovics, *IEEE Trans. Magn.*, 1988, **24**, 1892.
65. Y. H. Zheng, Y. Cheng, F. Bao and Y. S. Wang, *Mater. Res. Bull.*, 2006, **41**, 525.
66. R. Vijayakumar, Y. Koltypin, I. Felner and A. Gedanken, *Mat. Sci. Eng. A - Struct*, 2000, **286**, 101.
67. R. H. Kodama, A. E. Berkowitz, E. J. McNiff and S. Foner, *Phys. Rev. Lett.*, 1996, **77**, 394.
68. Y. Hernandez, V. Nicolosi, M. Lotya, F. Blighe, Z. Sun, S. De, I.T. McGovern, B. Holland, M. Byrne, Y. Gunko, J.J. Boland, P. Niraj, G. Duesberg, S. Krishnamurthy, R. Goodhue, J. Hutchison, V. Scardaci, A.C. Ferrari, J.N. Coleman, *Nat. Nanotechnol*. 2008, **3**, 563.
69. A. Policicchio, T. Caruso, G. Chiarello, E. Colavita, V. Formoso, R.G. Agostino, T. Tsoufis, D. Gournis, S. La Rosa, *Surf. Sci.*, 2007, **13**, 2823.

